Full Length Article

Luminescence and photoconversion properties of Ce-doped Ca₃Sc₂Si₃O₁₂ crystal☆

A. Shakhno [a,b,*], W. Gieszczyk [c], P. Bilski [c], S. Witkiewicz-Łukaszek [a], Tetiana Zorenko [a], M. Cieszko [b], Z. Szczepański [b], A. Kotlov [d], Yu Zorenko [a,**]

[a] Department of Physics, Kazimierz Wielki University in Bydgoszcz, 85090, Bydgoszcz, Poland
[b] Mechantronics Department, Kazimierz Wielki University in Bydgoszcz, 85-074, Bydgoszcz, Poland
[c] Institute of Nuclear Physics Polish Academy of Sciences in Krakow, 31345, Krakow, Poland
[d] Deutsches Elektronen-Synchrotron (DESY), 22607, Hamburg, Germany

ARTICLE INFO

ABSTRACT

This work is dedicated to investigation of the luminescent properties of the prospective photoconversion material based on the crystal of Ce^{3+} doped $Ca_3Sc_2Si_3O_{12}$ (CSSG) garnet. The GSSG:Ce crystal was grown using the micro-pulling-down (μPD) method. The CSSG:Ce crystal exhibited an intensive photoluminescence (PL) emission band with two sub-bands peaked at 504 and 545 nm, corresponding to 5d-4f ($^2F_{5/2;7/2}$) transitions. Furthermore, we have investigated also the formation of cerium multicenters in the GSSG:Ce crystal using analyses of the structure of Ce^{3+} photoluminescence emission and excitation spectra under excitation of the luminescence of this crystal by synchrotron radiation. The formation of Ce^{3+}-multicenters in CSSG:Ce garnet is caused by the local in-homogeneity of the dodecahedral sites of garnet lattice due to localization of the hetero-valent Sc^{3+} and Si^{4+} cations in the octahedral and tetrahedral positions of the garnet host. The existence of Ce^{3+} multicenters resulted in a significant enhancement of the Ce^{3+} emission band in the red range and improving the performance of conventional YAG:Ce phosphor. The next task of our work was to evaluate the possibility of application of the GSSG:Ce crystal as a light phosphor-converter (pc) for white light-emitting diodes (WLEDs). In the frame of this task, we have successfully developed a prototype of WLED by employing the CSSG:Ce crystal as a phosphor-converter (pc) with blue 450 emitting LED as well as investigated the color characteristics of this pc-WLED.

1. Introduction

White light-emitting diodes are widely adopted for lighting applications due to their remarkable attributes, including high efficiency, extended operational lifetime, and environmental sustainability compared to conventional light sources. The prevalent configuration of WLEDs involves combining blue LED chips with yellow-emitting Ce^{3+} doped $Y_3Al_5O_{12}$:Ce (YAG:Ce) garnet phosphor converters (pc). However, despite the good thermal stability of the Ce^{3+} luminescence in YAG:Ce at high temperatures, the absence of a red-emitting component in YAG:Ce phosphor converters requires the exploration of alternative

phosphors [1]. Therefore, there is a growing interest in identifying and developing alternative phosphor materials to address the above limitation in order to enhance the color rendering capabilities of pc-WLEDs.

The $Ca_3Sc_2Si_3O_{12}$:Ce (CSSG:Ce) silicate garnet emerges as an interesting alternative phosphor to YAG:Ce [2–6]. These phosphors demonstrate a high quantum yield what allows efficient conversion of excitation energy into emitted light. Additionally, they possess broadband emission spectra, allowing for a wide range of visible light emission [7]. Moreover, silicate garnet phosphors, including CSSG:Ce, exhibit excellent thermal stability of luminescence, making them well-suited for applications requiring elevated temperatures. Their

---

application as alternative phosphors offer promising prospects for enhancing the performance and versatility of lighting technologies.

Practical application of the CSSG:Ce garnet holds vast potential in various forms such as crystal, single-crystalline film (SCF), micropowder (MP) and nanopowder (NP). These forms enable the creation and development also cathodoluminescent materials, scintillators, lasers, and pc-WLEDs. The ongoing advancements in this phosphor type present promising opportunities within the field of semiconductor lighting technology. Consequently, a comprehensive investigation of the optical and structural properties of CSSG:Ce garnet is being strongly required [2,6,8–10].

This study focuses on the growth of Ce^{3+}-doped CSSG:Ce crystal by the micro-pulling-down method and investigation of their structural and luminescent properties using conventional optical methods and advanced luminescent spectroscopy under synchrotron radiation (SR) excitation. Furthermore, we have also investigated the color characteristics and phosphor conversion capabilities of WLED prototypes based on the CSSG:Ce crystal converters with varying thickness ranging from 0.8 to 1 mm. Our objective is to gain insights into the performance and potential of CSSG:Ce crystal as a phosphor converter for high-power WLED applications.

2. The growing technique and experimental techniques

The Ce^{3+}-doped CSSG crystal was grown through a micro-pulling-down method at the Institute of Nuclear Physics of Polish Academy of Sciences in Krakow, Poland. This method allowed the growth of the crystal from a molten state, resulting in the formation of a high-quality garnet crystal doped with Ce^{3+} ions. The CaO (Merck), Sc_2O_3 (Sigma-Aldrich), SiO_2 (Merck) and CeO_2 (Sigma-Aldrich) raw powders with a purity of 99.99 % were used. Stoichiometric amounts of CaO, Sc_2O_3, and SiO_2 were thoroughly mixed in the agate mortar to prepare a batch material for crystal growth experiments. To achieve Ce-doped CSSG crystal samples, CO_2 oxide in a concentration of 1 mol %, was employed as an admixture.

The prepared batch material, weighing 1.5 g, was loaded into a molybdenum crucible positioned directly on the graphite substrate following the heating process. To establish a suitable temperature gradient within the crystal growth area, three layers of ceramic thermal insulations composed of alumina and magnesium-stabilized zirconium dioxide were implemented. The closed chamber of the micro-pulling-down (μPD) furnace underwent an initial evacuation process, reducing the pressure to approximately 3.1 μbar. Then the chamber was filled with an inert gas (argon) to achieve the normal pressure. The crystal growth process occurred at a consistent pulling rate of 1.5 mm/min, utilizing an Al_2O_3 crystal as a seed. Throughout the entire growth experiment, the volumetric flow rate of argon remained at approximately 20 l/min.

To characterize the properties of the CSSG:Ce crystal under study, various structural and spectroscopic techniques were employed. The structural properties of these CSSG:Ce crystal samples were investigated using X-ray microtomography with a resolution of 0.5 μm (SkyScan 1272 spectrometer). The real composition of SCF samples was determined using a KEYENCE's Digital Microscope VHX-7000 (Mechelen, Belgium). Cathodoluminescence (CL), photoluminescence (PL), emission and PL excitation spectra (PLE), as well as PL decay kinetics were used for the characterization of the luminescent properties of the CSSG:Ce crystal. The CL spectra were obtained at room temperature (RT) using a scanning electron microscope (SEM, JSM-6390LV, JEOL Ltd., Tokyo, Japan), which was equipped with a Stellar Net spectrometer featuring a cooled TE-detector CCD that operated within the 200–1200 nm range. PL emission and excitation spectra, along with PL decay kinetics, were measured using an FS-5 spectrometer (Edinburg Instruments Ltd., Livingston, United Kingdom). Additionally, the luminescence of CSSG:Ce crystal sample was investigated at 12 K under synchrotron radiation excitation with energy in the 3.6–15 eV range at the Superlumi station at

HASYLAB (DESY, Hamburg). Photoconversion spectra measurements CSSG:Ce crystals with thickness in the 0.8–1 mm rage were performed using an AvaSpec-ULS 2048-LTEC fiber-optic spectrophotometer and an AvaSphere-50-IRRAD integrating sphere.

3. Structural properties

The radial deviation of the CSSG:Ce crystal content was established using a KEYENCE Digital Microscope VHX-7000. This device was equipped with a Laser-based Elemental Analyzer to enable instantaneous analysis of the material. The results of this analysis are shown in Table 1. The analysis of encompassed measurements was taken at five different points on the crystal sample, with ensuing averaging of the results to enhance accuracy of the content determination. The obtained results show some advance of Ca^{2+} and Si^{4+} cations and deficit of Sc^{3+} ions in comparison with stochiometric content of the $Ca_3Sc_2Si_3O_{12}$ garnet. For compensation of the charge excess, the cation vacancies V_{Sc} and Ca_{Sc} antisite defects can be created. However, such an assumption needs the detailed confirmation using EPR or other sensitive methods.

Furthermore, X-ray microtomography was used to investigate the internal structure of the $Ca_3Sc_2Si_3O_{12}$:Ce crystal, specifically to detect the existence of microdefects and phases different from the primary garnet phase. Visualization of these studies is presented in Fig. 1. It can be seen that the central part of the crystal consists of one dominant CSSG garnet phase. However, a secondary phase can be also observed at the edges of the crystal. The presence of the second phase at the crystal edges can be explained by the specific conditions of the crystal growth using the MPD method. The presence of other phases along the edges is a typical phenomenon and can be attributed to the specific growth conditions and solidification process, especially at the walls of crucible. During the MPD process, a crystal is grown by slowly pulling a seed crystal through a melt of the desired material. This controlled solidification allows the crystal to be formed from the molten material as it cools and crystallizes. However, certain factors can contribute to the formation of secondary phases, especially along the edges of the crystal. These factors can include thermal gradients, impurity concentration, solidification dynamics, segregation effects and crystallographic mismatch. In our case, we assume that the secondary phase at the edges of the crystal is formed due to overheating the melt at crucible walls and some segregation effects. To be more precise, differences in the density and composition of the material lead to segregation during solidification. Therefore, we can observe formation of the perovskite or other phase at the edges of the crystal with higher temperature of melting than that of the garnet. As a result of this circumstance, specifically, the existence of a secondary phase along the crystal's edges, *optical investigations of the crystal were exclusively conducted on its central part.*

4. Luminescent properties

4.1. Cathodoluminescence spectra

Fig. 2 shows the CL spectrum of the Ce^{3+}-doped $Ca_3Sc_2Si_3O_{12}$ crystal sample. This spectrum exhibits the characteristic double emission bands centered at 508 nm and 539 nm, corresponding to the 5 $d^1 \rightarrow$ 4f ($^2F_{5/2;\,7/2}$) transitions of Ce^{3+} ions in dodecahedral positions of the garnet host

Table 1
The nominal composition (in oxide powders) and the actual composition (in the crystal) of CSSG:Ce crystal grown via the MPD method.

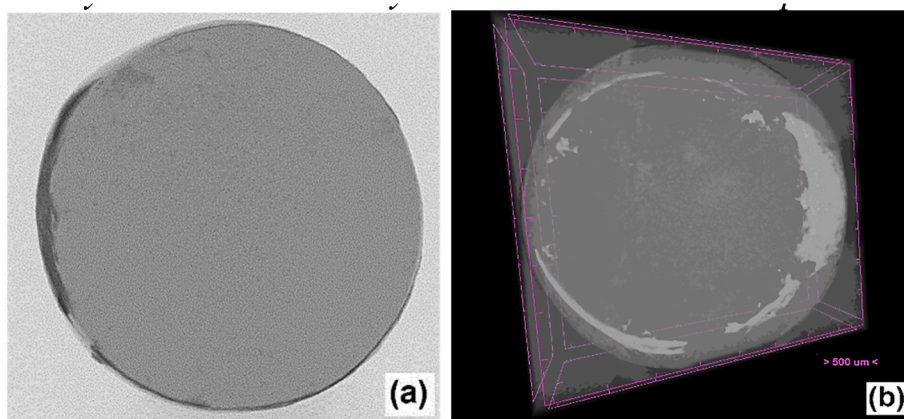|	Nominal crystal content	Actual crystal content
1	$Ca_3Sc_2Si_3O_{12}$:Ce	$Ca_{3.45}Sc_{1.37}Si_{3.18}O_{12}$:Ce
2	$Ca_3Sc_2Si_3O_{12}$:Ce	$Ca_{3.37}Sc_{1.43}Si_{3.2}O_{12}$:Ce
3	$Ca_3Sc_2Si_3O_{12}$:Ce	$Ca_{2.97}Sc_{1.21}Si_{3.82}O_{12}$:Ce
4	$Ca_3Sc_2Si_3O_{12}$:Ce	$Ca_{2.92}Sc_{1.12}Si_{3.96}O_{12}$:Ce
5	$Ca_3Sc_2Si_3O_{12}$:Ce	$Ca_{2.49}Sc_{1.25}Si_{4.26}O_{12}$:Ce
Average	$\mathbf{Ca_3Sc_2Si_3O_{12}}$:**Ce**	$\mathbf{Ca_{3.04}Sc_{1.28}Si_{3.68}O_{12}}$:**Ce**

Fig. 1. The radiograph of the sample acquired through X-ray tomography is depicted in (a), while the reconstructed three-dimensional image of the CSSG:Ce crystal structure is presented in (b).
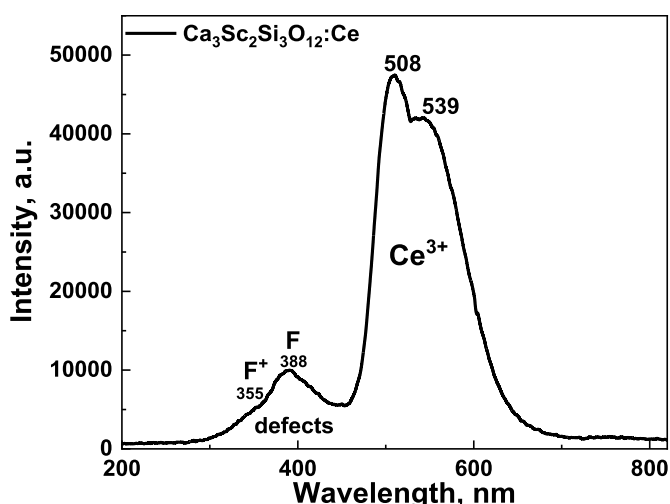

Fig. 2. RT CL spectrum of the CSSG:Ce crystal sample.

[4,7]. Generally, Fig. 2 illustrates the impact of substitution of Y^{3+} and Al^{3+} cations with Ca^{2+}, Sc^{3+}, and Si^{4+} cations in the dodecahedral, octahedral, and tetrahedral positions of the $Y_3Al_5O_{12}$ garnet host. This causes a significant shift of the maximum of the Ce^{3+} emission band towards the blue range from 540 to 508 nm compared to the YAG:Ce single crystal [11]. is observed due to substitution of Y^{3+} cations with Ca^{2+} ions in the dodecahedral positions, Al^{3+} cations with Sc^{3+} cations in the octahedral sites and Al^{3+} cations on Si^{4+} ions in the tetrahedral positions of the garnet host. The overall influence of such type substitution results in the presence of smaller crystal field strengths in the different dodecahedral sites of the CSSG garnet lattice, where the Ce^{3+} ions are located.

In addition to the luminescence emitted by Ce^{3+} ions, there are other high-energy emission bands are present in the CL spectrum of CSSG:Ce crystal. Particularly, the wide bands are observed in the ultraviolet (UV) range with maxima at 355 and 388 nm. Similar broad low-intensity bands in the UV range are observed in Ca^{2+}-Si^{4+} and Mg^{2+}-Si^{4+}-based garnets and these bands typically have been associated with the luminescence of defect centers [12–16]. Namely, the nature these two UV bands can be attributed to the luminescence of F- and F^+ centers, respectively, due to high concentration of oxygen vacancies in the Ca^{2+}-Mg^{2+}-Si^{4+} based garnets [12–16]. The presence of these charged vacancies may be caused by variations in the Ca^{2+} and Si^{4+} content, as well as by need for local charge compensation of the excess of one cations during the crystal growth in an oxygen-free atmosphere [17,18].

4.2. Photoluminescence spectra and Ce^{3+} multicenter formation

Under excitation with 400 nm light, the PL spectrum of the CSSG:Ce crystal (Fig. 3a) consists of the typical double Ce^{3+} 5d-4f emission bands, peaked at 501 and 536 nm, corresponding to the transitions from the lowest $5d_1$ level to the two spin-orbit components $^2F_{5/2,7/2}$ (separated by ~2000 cm^{-1}) of the ground state (Fig. 3a). However, under excitation with different wavelengths in the 400–450 nm range, these bands are notably shifted to the red range and maxima of the double bands are located at 507 and 542 nm for 460 nm excitation, primarily associated with distinct Ce1 and Ce2 centers, respectively. The red shift in the primary maxima of the PL spectra and variations in intensity at the peak positions of CSSG:Ce crystal occur in a non-monotonic way with increasing excitation wavelength (Fig. 3c), as opposed to the absence of the mentioned changes for the YAG:Ce reference crystal (not presented in Fig. 3c) [4,7].

The PLE spectra of CSSG:Ce crystal are illustrated in Fig. 3b. The PLE spectra of luminescence show a set of broad bands located in the blue-green range. Within the wavelength range of 250–550 nm, multiple sets of excitation bands are observed. Notably, the strongest E1 (440 nm) and E2 (310 nm) bands, can be attributed to the 4f−5d (E_g and T_{2g}) transitions of the primary Ce1 center, agreeing with the results of prior research [4,19,20]. Similarly, additional sets of excitation bands, E1' (457 nm) and E2' (331 nm), can be associated with the $4f_1{\rightarrow}5d_1$ transitions of the secondary Ce2 centers. These centers exhibit distinct local environments when compared to the Ce1 center. Additionally, the excitation band peaking at 361 nm possibly corresponds to a defect center, most probably the F^+ center [4].

The decay kinetic profiles of the Ce^{3+} luminescence in the CSSG:Ce crystal, registered at the range 490–570 nm under excitation at 450 nm, are shown in Fig. 3d. Similar to other Ca^{2+}-Si^{4+} garnets based [21–23], the decay kinetics of Ce^{3+} emission in CSSG:Ce crystals exhibit a strong non-exponential behavior. Due to this, a three-exponential fit of the decay curves, given by equation $I = \Sigma A_i * exp(-t/\tau_i)$, was used to qualitatively desertions of the luminescence timing profiles. In spite of the fact that a three-exponential approximation does not fully describe the luminescence decay in cases of quenching via energy transfer, the decay time values can be considered as estimations for the luminescence decay times of respective Ce^{3+} multicenters (Table 2). Specifically, the luminescence decay kinetics of the CSSG:Ce crystal, measured at the appropriate wavelengths (namely, at 490 nm and 570 nm), are manifested by three components τ_i, where i = 3, each with a unique decay time associated with distinct Ce1 and Ce2 centers. In particular, the decay times ($\tau1$, $\tau2$ and $\tau3$) of the Ce1 center emission in the CSSG:Ce crystal, recorded at 490 nm under excitation at 450 nm, are equal to 3.7 ns, 21.7 ns and 64.0 ns when the luminescence decay times of Ce2
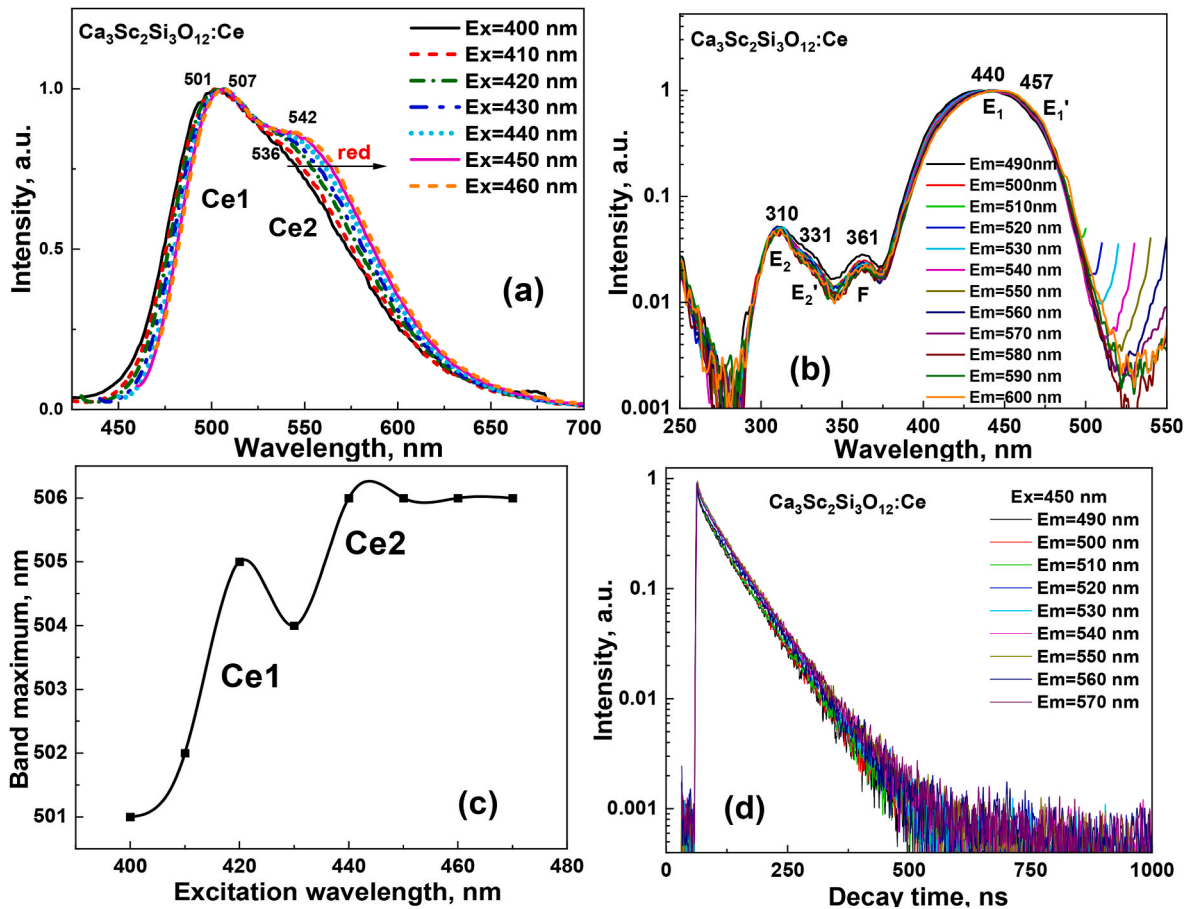
Fig. 3. Details of the luminescent properties of CSSG:Ce crystal at RT. Emission (a) and excitation (b) spectra were recorded in different parts of the respective Ce^{3+} emission/excitation bands. (c) - dependences of the maxima in the peak positions of Ce^{3+} emission bands on the excitation wavelength in CSSG:Ce crystal. (d) PL decay kinetics at RT were recorded under blue light (450 nm) excitation in different parts of the Ce^{3+} emission band.

Table 2
Parameters of three exponential approximation of the decay curves presented in Fig. 3d.

Emission wavelength, nm	t_1, ns	A_1	t_2, ns	A_2	t_3, ns	A_3
490	3.7	148.7	21.7	426.4	64.0	1762.4
500	3.7	144.2	21.7	423.3	64.0	1760.8
510	4.9	1125.7	37.0	1212.1	69.9	2130.8
520	4.8	828.8	27.4	862.8	65.9	2759.4
530	5.8	662.2	31.5	854.6	67.0	2866.9
540	4.4	1005.8	31.8	1169.4	69.1	2828.5
550	3.5	596.4	26.3	820.6	67.4	2865.8
560	2.3	543.9	20.9	382.1	66.9	1569.4
570	5.0	754.7	44.8	1757.8	76.5	1942.3

Table 3
Spectral characteristics of the different Ce^{3+} multicenters in $Ca_3Sc_2Si_3O_{12}$:Ce garnet.

Type of centers	Maximum of dominant emission bands, nm	Position of E2 and E1 excitation bands, nm	$\Delta E = E_2 - E_1$, eV	Stokes shift, eV
Ce1	501; 536	312; 434	1.117	0.382
Ce2	506; 542	309; 446	1.233	0.330

center, recorded at 570 nm under the same excitation, is significantly large and amounts to 5.0 ns, 44.8 ns and 76.5 ns (see Table 2).

This behavior of the decay curves in CSSG:Ce crystal may also indicate a possible energy transfer from high-energy to low-energy Ce^{3+} centers in this garnet [19,20,24]. Different decay times can correspond to different Ce^{3+} centers in the dodecahedral sites of $Ca_3Sc_2Si_3O_{12}$ garnet host with various local environments with oxygen ions cations due to the local inhomogeneity at localization of Sc^{3+} and Si^{4+} ions in octahedral and tetrahedral sites, respectively [7].

Spectral characteristics of the different Ce^{3+} multicenters in CSSG:Ce crystal are summarized in Table 3.

5. Low-temperature luminescence under synchrotron radiation

The luminescent properties of the $Ca_3Sc_2Si_3O_{12}$:Ce crystal were investigated also at 12 K under excitation by SR with an energy in the 3.7–20.6 eV range at the new Superlumi station located at P66 beamline at PETRA storage ring at DESY (Hamburg, Germany) [25]. The PL emission and excitation spectra as well as the PL decay kinetics were measured in time gate between SR pulses with a repetition time of 16 ns and a duration of 0.127 ns.

The emission spectra of $Ca_3Sc_2Si_3O_{12}$:Ce crystal are shown in Fig. 4. The dominant double luminescence bands peaked in the green-yellow range are related to the $5d^1 \rightarrow 4f$ ($^2F_{5/2,7/2}$) transitions of Ce^{3+} ion in this garnet host. Meanwhile, with increasing the excitation wavelength from 20.64 eV (60 nm) to 4.13 eV (300 nm), the position of emission band of the CSSG:Ce crystal shows the red shift from 493 to 502 nm firstly and then the blue shift from 502 nm to 498 nm (Fig. 4, Table 4). Therefore, the shift of the main maxima of the PL spectra of the CSSG:Ce crystal occurs non-monotonically with increasing the excitation
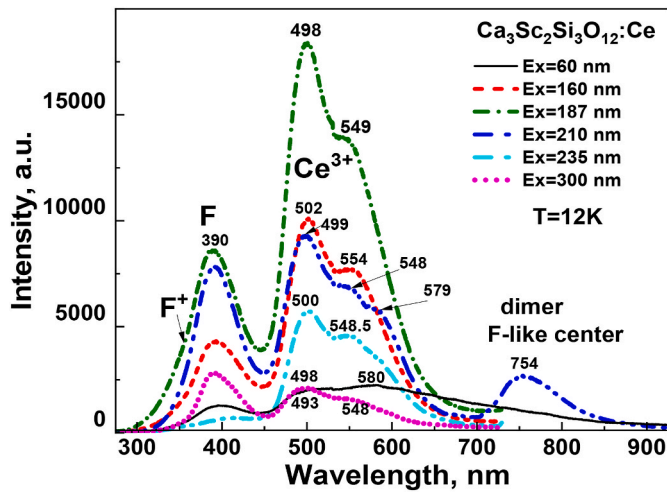
Fig. 4. Luminescence spectra of CSSG:Ce crystal at 12 K under excitation by SR in the interband transition range at 20.63 eV (60 nm) (1), exciton range at 7.74 eV (2) and 6.62 eV (187 nm) (3) as well as in the range of defect band at 5.895 eV (210 nm) (4) and Ce^{3+} absorption band at 5.27 eV (235 nm) (5) and 4.13 eV (300 nm) (6).

Table 4
Spectral characteristics of the different Ce^{3+} multicenters in CSSG:Ce crystal.

Excitation energy, eV	Position of emission bands, nm		Additional bands, nm
20.63	493	580	580
7.74	502	554	
6.62	498	549	
5.89	499	548	579
5.27	500	548.5	
4.13	498	548	

wavelength. Furthermore, the additional peaks at 579–580 nm are well resolved under excitation at 20.64 eV (60 nm) in the range of interband transitions and defect-related band at 5.895 eV (210 nm). Such a behavior of the PL emission spectra clearly indicates the Ce^{3+} multi-center formation in CSSG:Ce garnet. Therefore, the emission spectra of the CSSG:Ce crystal under excitation at the different wavelengths, demonstrate overlapped two pairs of the Ce^{3+} emission bands peaked mainly at 493–502 nm and 548–554 nm ranges (Fig. 4), related to the different Ce1 and Ce2 centers [4,7,26].

Apart from the luminescence of Ce^{3+} ions, other emission bands in the UV range are also present in the emission spectra of CSSG:Ce crystal. The main UV band are peaked at 390 nm in CSSG:Ce crystal. However, the high-energy wing of this band is notably elongated due to the presence of another high-energy emission band of F^+ centers peaked at 355 nm. Taking into account published data on the luminescence of charged oxygen vacancies in the different oxide compounds [4,7,27], the complex UV emission bands with sub-bands peaked in the 388–390 nm and 355–360 nm ranges can correspond to the luminescence of F^+ and F centers (one and two charged oxygen vacancies, respectively) in the garnet hosts. Another low intensity luminescence band peaking at 590 nm on the low-energy wind of Ce^{3+} emission band and well resolved band peaked at 754 nm can be related to the different dimmer or more complicated centers, based on the couples of F^+ and F centers in CSSG host (Fig. 4) [28].

The excitation spectra of Ce^{3+} and defect luminescence in CSSG:Ce crystal in the 60–334 nm (20.7–3.7 eV) range at 12 K, are shown in Fig. 5. Several sets of excitation bands are distinguished in the 3.5–10 eV range. The broad absorption band centered at 5.22 eV (238 nm) is due to $4f \rightarrow 5d_3$ absorption transition of Ce^{3+} ions. The strong bands in the exciton range correspond to creation of excitons bound with different Ce^{3+} centers. Furthermore, some difference in the positions of these
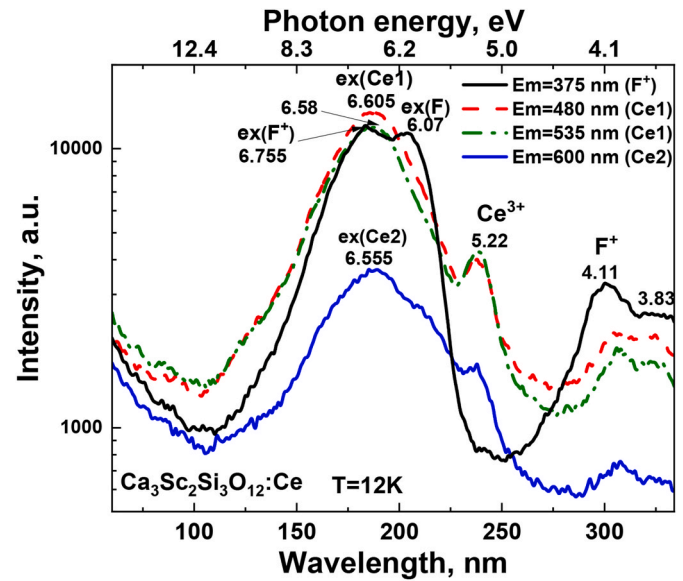

Fig. 5. Excitation spectra of Ce^{3+}-centers in CSSG:Ce crystal at 12 K in the 334-60 nm range (20.66–3.71 eV), monitored at 375 nm (1), 480 nm (2), 535 nm (3) and 600 nm (4).

excitation bands at registration of the Ce^{3+} luminescence at 480–530 nm range and at 600 nm enables the correct determination of the energy creation of excitons bound with Ce1 and Ce2 centers which is equal to 6.605 eV and 6.555 eV, respectively. The notable increase of the intensity of Ce^{3+} luminescence and other emission centers as well in 12–20.6 eV range (Fig. 5b) is caused by the multiplication of the electronic excitations in this energy range [27–31].

The excitation band for luminescence of defect centers, recorded at 375 nm in CSSG:Ce crystal, is mostly associated with intrinsic transitions of F^+ centers in the bands peaked at 323 nm (3.83 eV) and 256 nm (4.83 eV), respectively. Additionally, the prominent band peaked at 183 nm (6.755 eV) in the exciton range aligns with the energy of creation of an excitons bound to this center followed by the electron-hole recombination on these defects [32–34]. However, the strong band peaked at 205.5 nm (6.02 eV) in this excitation spectrum is rather correspond to the F center luminescence and most probably is related to the creation of an exciton bound with F centers. The support of this conclusion is connected with substantial differences in the decay kinetics of the luminescence at 375 nm under excitation in 205.5 nm (6.02 eV) band in comparison with the decay kinetics under excitation in the 323 nm (3.83 eV) and 256 nm (4.83 eV) bands of F^+ centers.

The decay kinetic profiles corresponding to the F and F^+ center luminescence in the CSSG:Ce crystal, recorded at 375 nm, are shown in Fig. 6. Similarly to other Ca^{2+}-Si^{4+} based garnets, the non-exponential decay kinetics of the F^+ center emission most probably is caused by the energy transfer to Ce^{3+} ions. Namely, the values of decay times of the F^+ luminescence in CSSG:Ce crystal, registered at 375 nm under excitation in the 301 nm (4.11 eV) and 323 nm (3.83 eV) bands, are equal to $\tau_2 = 7.2$ ns and $\tau_3 = 4.9$ ns, respectively. Such a behavior of the decay curves of the F^+ center luminescence in the CSSG:Ce crystal can also indicate the possible energy transfer both to high-energy or low-energy Ce^{3+} emitting centers in this garnet. The different decay times of the F^+ center luminescence in the CSSG:Ce crystal can correspond to the excitation of different Ce^{3+} centers in the dodecahedral positions of the garnet lattice with various local surroundings by oxygen and cations (Sc^{3+} and Si^{4+} ions in the octahedral and tetrahedral positions, respectively) [7]. However, the decay profiles of the dominant F center luminescence (Fig. 6) present the fast component with a decay time of $\tau_1 = 2.21$ ns, related to the allowed transitions from singlet excited level and the second slow component corresponding to the partly allowed
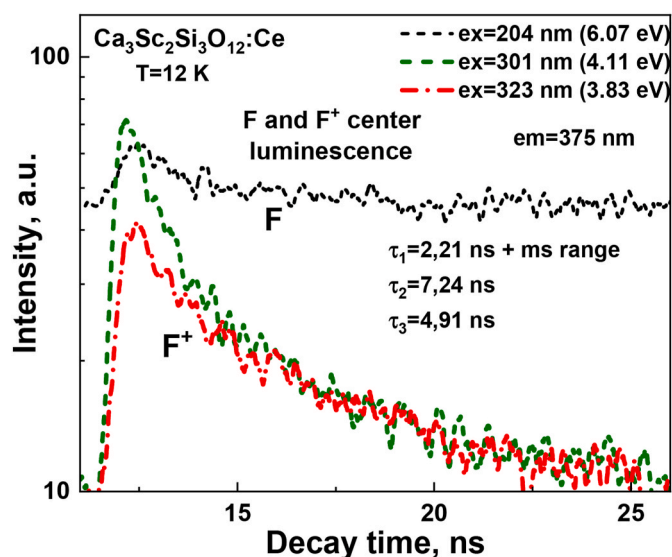
Fig. 6. Decay kinetics of F^+ and F centers luminescence in CSSG:Ce crystal at 12 K under excitation by SR with different wavelengths in the characteristic points of excitation spectra in Fig. 5.

transition in this center from the triplet relaxed level [7,12–16].

6. Photoconversion properties

In order to show the potential applications of the CSSG:Ce crystal phosphor, prototypes of cool white light-emitting diodes (WLEDs) were developed. These WLED prototypes utilized CSSG:Ce crystal phosphor-converters (pc) with varying thickness ranging from 1 to 0.8 mm. These phosphor-converters were coupled with GaN 432 nm blue emitting LED chips. The emission spectrum of these WLEDs covers the visible range, producing cool white light spanning from 458 to 688 nm. Additionally, Fig. 7 illustrates the connection between the photoconverter properties of the CSSG:Ce crystal and the sample's thickness. Notably, as the pc-thickness increases, there is a reduction in the intensity of the blue LED emission, accompanied by a raising in the intensity of the green-yellow emission band. This green-yellow emission reaches its maximum intensity at an approximate thickness of 1.0 mm. We assume that at further increasing the sample thickness beyond 1 mm, it becomes possible to obtain emissions much closer to white light. This has the potential to lead to the achievement of a nearly perfect cool white light emission with large CCC and CRI values.

In Fig. 7b, the CIE-1931 chromaticity diagram shows the shift in color coordinates (x, y) of the CSSG:Ce crystal across various thicknesses ranging from 0.8 to 1.0 mm. Notably, these coordinates follow a non-linear pattern, with both x and y values as well as CRI and LE values increasing as the thickness of the sample grows. The CIE chromaticity coordinates of the WLED prototypes are detailed in Table 5.

7. Conclusions

The $Ca_3Sc_2Si_3O_{12}$ crystal doped with Ce^{3+} was grown using the µPD method. The actual content of the grown crystal was probed through EDS analysis. Additionally, X-ray microtomography was employed to examine the internal structure of the crystal, specifically targeting the identification of secondary phases distinct from the primary garnet phase.

The luminescence characteristics of the $Ca_3Sc_2Si_3O_{12}$:Ce crystal were explored using conventional cathodoluminescence and photo-luminescence as well as luminescent spectroscopy under excitation by synchrotron radiation with energy in the 3.7–20 eV range. The 5d - 4f transitions of Ce^{3+} ions were identified in the form of the dominant emission band both in cathodoluminescence and photoluminescence spectra. The luminescence of F^+ and F center is also observed in the CL and PL spectra in the UV range.

We have also observed the formation of at least two Ce^{3+} centers (Ce1 and Ce2) in the emission and excitation spectra as well as in the decay kinetics of the Ce^{3+} luminescence of $Ca_3Sc_2Si_3O_{12}$:Ce crystal. Such Ce^{3+} centers possess different spectral behaviors (the positions of the emission and excitation bands as well as the PL decay kinetics) due to the different local surroundings and crystal field strength of the respective dodecahedral positions of the garnet host. Such an in-homogeneity of local environment of the dodecahedral positions of the garnet host is caused by the substitution of the octahedral positions by

Table 5
CIE chromaticity coordinates, CTT and luminous efficiency of a WLED lamp fabricated on the base of 450 nm LED chip and CSGG:Ce crystals with different thicknesses.

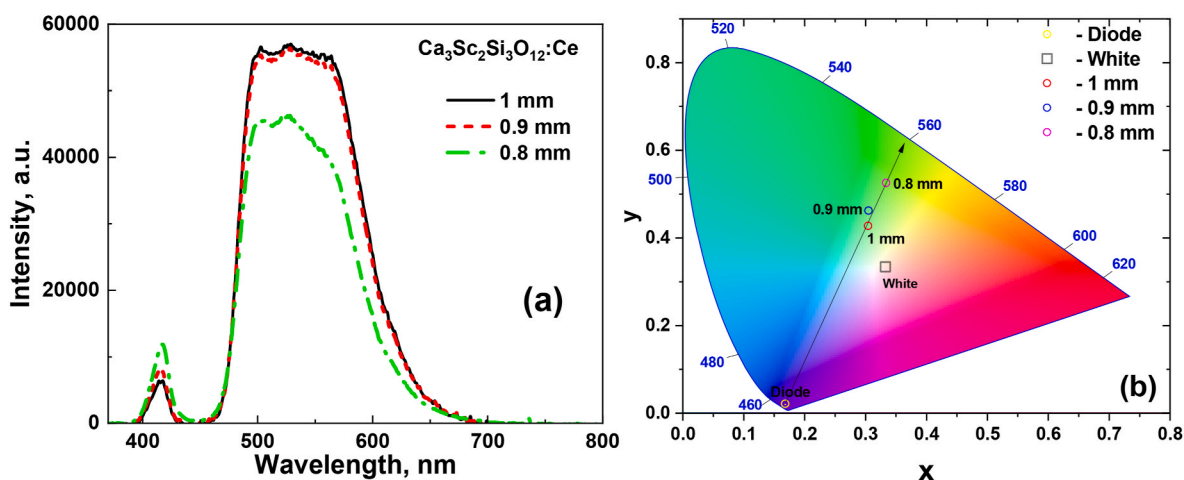| Thicknesses of the sample, mm	CIE Coordinates		CCT, K	CRI	LE, lm/W
	x	y			
0.8	0.4567	0.5299	3489	39.7	68
0.9	0.4498	0.5306	3580	46.1	81
1	0.4483	0.5341	3620	42.3	107

Fig. 7. The spectral characteristics of CSSG:Ce crystals combined with GaN 432 nm blue LED (a); the color coordinates of LEDs based on CSSG:Ce crystals with different thickness in the 0.8–1 mm range within the CIE-1931 color space chromaticity diagram (b).

heterovalent Sc^{3+} ions and the tetrahedral positions by Si^{4+} ions.

Based on the results of optical luminescence investigations, the characteristics of Ce1 and Ce2 center were estimated: the positions of dominant emission bands (501; 536 nm and 506; 542 nm at RT) and excitation bands (312; 434 nm and 309; 446 nm at RT), the Stokes shift (0.382 and 0.330 eV at RT), as well as the energy of creation of an excitons bound with Ce1 and Ce2 centers (6.605 eV and 6.555 eV at 12K), respectively. We have also determined the luminescent characteristics and energetic structure of F^+ and F centers in the CSSG host, including the energy of creation of excitons bound with F and F^+ centers being equal to 6.07 eV and 6.755 eV at 12K, respectively.

Finally, we have investigated the photoconversion properties of $Ca_3Sc_2Si_3O_{12}$:Ce crystals with different thicknesses ranging from 1.0 to 0.8 mm, combined with GaN 432 nm blue LED chip. We suggest that extending the sample thickness above 1 mm may result in emission that exhibits greater proximity to white light characteristics. This can ensure effective matching of different shades of white light devices.

Author contributions

Anna Shakhno performed the measurements and analyzation of the structural, optical and photoconversion properties of CSSG:Ce crystals and participated in the writing and preparation of paper; Mieczysław Cieszko and Zbigniew Szczepański performed structural measurements and analyzed their results; Wojciech Gieszczyk performed growth of the CSSG:Ce crystal; Paweł Bilski managed the crystal preparation; Sandra Witkiewicz-Łukaszek performed cathodoluminescence measurements; Tetiana Zorenko participated in measurements of PL, PLE, and decay kinetics of the samples; Alexei Kotlov supervised the measurements with synchrotron radiation; Yuriy Zorenko analyzed all experimental data and participated in writing and editing of the paper.

Institutional review board statement

Not applicable.

Informed consent statement

Not applicable.

Authors' agreement

We wish to confirm that there are no known conflicts of interest associated with this publication and there has been no significant financial support for this work that could have influenced its outcome.

We confirm that the manuscript has been read and approved by all named authors and that there are no other persons who satisfied the criteria for authorship but are not listed. We further confirm that the order of authors listed in the manuscript has been approved by all of us.

We confirm that we have given due consideration to the protection of intellectual property associated with this work and that there are no impediments to publication, including the timing of publication, with respect to intellectual property. In so doing we confirm that we have followed the regulations of our institutions concerning intellectual property.

2010.2023.

Anna Shakhno.

Declaration of competing interest

We wish to confirm that there are no known conflicts of interest associated with this publication and there has been no significant financial support for this work that could have influenced its outcome.

We confirm that the manuscript has been read and approved by all named authors and that there are no other persons who satisfied the criteria for authorship but are not listed. We further confirm that the order of authors listed in the manuscript has been approved by all of us.

We confirm that we have given due consideration to the protection of intellectual property associated with this work and that there are no impediments to publication, including the timing of publication, with respect to intellectual property. In so doing we confirm that we have followed the regulations of our institutions concerning intellectual property.

We understand that the Corresponding Author is the contact for the Editorial process (including Editorial Manager and direct communications with the office). He/she is responsible for communicating with the other authors about progress, submissions of revisions and final approval of proofs. We confirm that we have provided a current, correct email address which is accessible by the Corresponding Author and which has been configured to accept email from annshakhno@gmail. com; zorenko@ukw.edu.pl.

Signed by all authors as follows: A. Shakhno, W. Gieszczyk, P. Bilski, S. Witkiewicz-Łukaszek, Tetiana Zorenko, M. Cieszko, Z. Szczepański, A. Kotlov, Yu. Zorenko.

Data availability

Data will be made available on request.

References

[1] M. Xu, J. Chang, J. Wang, C. Wu, F. Hu, Al_2O_3-YAG:Ce composite ceramics for high-brightness lighting, Opt Express 27 (2019) 872, https://doi.org/10.1364/oe.27.000872.

[2] T. Kato, Y. Usui, G. Okada, N. Kawaguchi, T. Yanagida, X-ray induced luminescence properties of Ce-doped single crystal, Nucl. Instrum. Methods Phys. Res. Sect. A Accel. Spectrom. Detect. Assoc. Equip. 954 (2020), 161301, https://doi.org/10.1016/j.nima.2018.09.136.

[3] Y. Shimomura, T. Honma, M. Shigeiwa, T. Akai, K. Okamoto, N. Kijima, Photoluminescence and crystal structure of green-emitting $Ca_3Sc_2Si_3O_{12}$:Ce^{3+} phosphor for white light emitting diodes, J. Electrochem. Soc. 154 (2007) J35, https://doi.org/10.1149/1.2388856.

[4] V. Gorbenko, T. Zorenko, S. Witkiewicz, K. Paprocki, A. Iskaliyeva, A. M. Kaczmarek, R. Van Deun, M.N. Khaidukov, M. Batentschuk, Y. Zorenko, Luminescence of Ce^{3+} multicenters in Ca^{2+}-Mg^{2+}-Si^{4+} based garnet phosphors, J. Lumin. 199 (2018) 245–250, https://doi.org/10.1016/j.jlumin.2018.03.058.

[5] Y. Liu, X. Zhang, Z. Hao, Y. Luo, X. Wang, L. Ma, J. Zhang, Luminescence and energy transfer in $Ca_3Sc_2Si_3O_{12}$:Ce^{3+},Mn^{2+} white LED phosphors, J. Lumin. 133 (2013) 21–24, https://doi.org/10.1016/j.jlumin.2011.12.052.

[6] K.V. Ivanovskikh, A. Meijerink, F. Piccinelli, A. Speghini, E.I. Zinin, C. Ronda, M. Bettinelli, Optical spectroscopy of $Ca_3Sc_2Si_3O_{12}$, $Ca_3Y_2Si_3O_{12}$ and $Ca_3Lu_2Si_3O_{12}$ doped with Pr^{3+}, J. Lumin. 130 (2010) 893–901, https://doi.org/10.1016/j.jlumin.2009.12.031.

[7] I. Levchuk, A. Osvet, C.J. Brabec, M. Batentschuk, A. Shakhno, T. Zorenko, Y. Zorenko, Micro-powder $Ca_3Sc_2Si_3O_{12}$:Ce silicate garnets as efficient light converters for WLEDs, Opt. Mater. 107 (2020) 109978, https://doi.org/10.1016/j.optmat.2020.109978.

[8] Y. Chen, M. Gong, K.W. Cheah, Effects of fluxes on the synthesis of Ca3Sc2Si3O12:Ce3+ green phosphors for white light-emitting diodes, Mater. Sci. Eng., B 166 (2010) 24–27, https://doi.org/10.1016/j.mseb.2009.09.024.

[9] Y.-F. Wu, Y.-H. Chan, Y.-T. Nien, I.-G. Chen, Crystal structure and optical performance of Al^{3+} and Ce^{3+} codoped $Ca_3Sc_2Si_3O_{12}$ green phosphors for white LEDs, J. Am. Ceram. Soc. 96 (2012) 234–240, https://doi.org/10.1111/jace.12034.

[10] F. Piccinelli, A. Speghini, G. Mariotto, L. Bovo, M. Bettinelli, Visible luminescence of lanthanide ions in $Ca_3Sc_2Si_3O_{12}$ and Ca3Y2Si3O12, J. Rare Earths 27 (2009) 555–559, https://doi.org/10.1016/s1002-0721(08)60287-2.

[11] S.V. Nizhankovsky, A.Ya Dan'ko, O.V. Zelenskaya, V.A. Tarasov, YuV. Zorenko, V. M. Puzikov, L.A. Grin', A.G. Trushkovskii, V.P. Savchin, Cathodoluminescence and scintillation characteristics of YAG:Ce crystals grown by horizontal directional crystallization in a protective atmosphere, Tech. Phys. Lett. 35 (2009) 964–966, https://doi.org/10.1134/s1063785009100265.

[12] Z. Pan, Y. Xu, Q. Hu, W. Li, H. Zhou, Y. Zheng, Combination cation substitution tuning of yellow-orange emitting phosphor Mg2Y2Si2O12:Ce3+, RSC Adv. 5 (2015) 9489–9496, https://doi.org/10.1039/c4ra14425b.

[13] M. Raukas, J. Kelso, Y. Zheng, K. Bergenek, D. Eisert, A. Linkov, F. Jermann, Ceramic phosphors for light conversion in LEDs, ECS J. Solid State Sci. Technol. 2 (2012) R3168–R3176, https://doi.org/10.1149/2.023302jss.

[14] L.M. Chepyga, A. Osvet, I. Levchuk, A. Ali, Y. Zorenko, V. Gorbenko, T. Zorenko, A. Fedorov, C.J. Brabec, M. Batentschuk, New silicate based thermographic phosphors Ca3Sc2Si3O12:Dy, Ca3Sc2Si3O12:Dy,Ce and their photoluminescence properties, J. Lumin. 202 (2018) 13–19, https://doi.org/10.1016/j.jlumin.2018.05.039.

[15] V. Gorbenko, T. Zorenko, A.M. Kaczmarek, R. Van Deun, A. Fedorov, Y. Zorenko, Eu3+ multicenter formation and luminescent properties of Ca3Sc2Si3O12:Eu and Ca2YScMgSiO12:Eu single crystalline films, Opt. Mater. 90 (2019) 70–75, https://doi.org/10.1016/j.optmat.2019.02.030.

[16] L. Zhou, W. Zhou, F. Pan, R. Shi, L. Huang, H. Liang, P.A. Tanner, X. Du, Y. Huang, Y. Tao, L. Zheng, Spectral properties and energy transfer of a potential solar energy converter, Chem. Mater. 28 (2016) 2834–2843, https://doi.org/10.1021/acs.chemmater.6b00763.

[17] YuV. Zorenko, A.S. Voloshinovskii, G.M. Stryganyuk, I.V. Konstankevych, Ultraviolet luminescence of single crystals and single-crystal films of YAlO3, Opt. Spectrosc. 96 (2004) 70–76, https://doi.org/10.1134/1.1643988.

[18] A. Shakhno, A. Markovskyi, T. Zorenko, S. Witkiewicz-Łukaszek, Y. Vlasyuk, A. Osvet, J. Elia, C.J. Brabec, M. Batentschuk, Y. Zorenko, Micropowder Ca2YMgScSi3O12:Ce silicate garnet as an efficient light converter for white LEDs, Materials 15 (2022) 3942, https://doi.org/10.3390/ma15113942.

[19] J. Ueda, S. Tanabe, (INVITED) Review of luminescent properties of Ce3+-doped garnet phosphors: new insight into the effect of crystal and electronic structure, Opt. Mater. X 1 (2019), 100018, https://doi.org/10.1016/j.omx.2019.100018.

[20] V. Gorbenko, T. Zorenko, P. Pawlowski, A. Iskaliyeva, K. Paprocki, A. Suchocki, Ya Zhydachevskii, A. Fedorov, N. Khaidukov, R. Van Deun, F. Schröppel, A. Osvet, M. Batentschuk, Yu Zorenko, Luminescent and scintillation properties of Ce 3+ doped Ca 2 RMgScSi 3 O 12 (R = Y, Lu) single crystalline films, J. Lumin. 195 (2018) 362–370, https://doi.org/10.1016/j.jlumin.2017.11.052.

[21] A.A. Setlur, W.J. Heward, Y. Gao, A.M. Srivastava, R.G. Chandran, M.V. Shankar, Crystal chemistry and luminescence of Ce3+-doped Lu2CaMg2(Si,Ge)3O12 and its use in LED based lighting, Chem. Mater. 18 (2006) 3314–3322, https://doi.org/10.1021/cm060898c.

[22] M. Tyagi, F. Meng, M. Koschan, S.B. Donnald, H. Rothfuss, C.L. Melcher, Effect of codoping on scintillation and optical properties of a Ce-doped Gd3Ga3Al2O12 scintillator, J. Phys. D Appl. Phys. 46 (2013), 475302, https://doi.org/10.1088/0022-3727/46/47/475302.

[23] Y. Wu, F. Meng, Q. Li, M. Koschan, C.L. Melcher, Role of Ce4+ in the scintillation mechanism of codoped Gd3Ga3Al2O12:Ce, Phys. Rev. Appl. 2 (2014), https://doi.org/10.1103/physrevapplied.2.044009.

[24] N.M. Khaidukov, I.A. Zhidkova, N.Y. Kirikova, V.N. Makhov, Q. Zhang, R. Shi, H. Liang, Mechanism for bifurcation of broadband luminescence spectra from Ce 3 + ions at dodecahedral sites in garnets {CaY 2 }[M 2](Al 2 Si)O 12 (M = Al, Ga, Sc), Dyes Pigments 148 (2018) 189–195, https://doi.org/10.1016/j.dyepig.2017.09.012.

[25] V. Pankratov, A. Kotlov, Luminescence spectroscopy under synchrotron radiation: from SUPERLUMI to FINESTLUMI, Nucl. Instrum. Methods Phys. Res. Sect. B Beam Interact. Mater. Atoms 474 (2020) 35–40, https://doi.org/10.1016/j.nimb.2020.04.015.

[26] A. Yoshikawa, V. Chani, Growth of optical crystals by the micro-pulling-down method, MRS Bull. 34 (2009) 266–270, https://doi.org/10.1557/mrs2009.77.

[27] YuV. Zorenko, A.S. Voloshinovskiĭ, I.V. Konstankevych, Luminescence of F + and F centers in YAlO3, Opt. Spectrosc. 96 (2004) 532–537, https://doi.org/10.1134/1.1719141.

[28] Yu Zorenko, K. Fabisiak, T. Zorenko, A. Mandowski, Q. Xia, M. Batentschuk, J. Friedrich, G. Zhusupkalieva, Comparative study of the luminescence of Al2O3:C and Al2O3 crystals under synchrotron radiation excitation, J. Lumin. 144 (2013) 41–44, https://doi.org/10.1016/j.jlumin.2013.06.043.

[29] T. Zorenko, V. Gorbenko, A. Petrosyan, W. Gieszczyk, P. Bilski, Yu Zorenko, Intrinsic and defect-related luminescence of YAlO3 and LuAlO3 single crystals and films, Opt. Mater. 86 (2018) 376–381, https://doi.org/10.1016/j.optmat.2018.10.029.

[30] P.A. Tanner, L. Fu, L. Ning, B.-M. Cheng, M.G. Brik, Soft synthesis and vacuum ultraviolet spectra of YAG:Ce3+ nanocrystals: reassignment of Ce3+ energy levels, J. Phys. Condens. Matter 19 (2007), 216213, https://doi.org/10.1088/0953-8984/19/21/216213.

[31] V. Gorbenko, T. Zorenko, K. Paprocki, A. Iskaliyeva, A. Fedorov, F. Schröppel, I. Levchuk, A. Osvet, M. Batentschuk, Yu Zorenko, Epitaxial growth of single crystalline film phosphors based on the Ce3+-doped Ca2YMgScSi3O12 garnet, CrystEngComm 19 (2017) 3689–3697, https://doi.org/10.1039/c7ce00630f.

[32] V. Gorbenko, T. Zorenko, S. Witkiewicz-Łukaszek, A. Shakhno, A. Osvet, M. Batentschuk, A. Fedorov, Y. Zorenko, Crystallization and investigation of the structural and optical properties of Ce3+-doped Y3−xCaxAl5−ySiyO12 single crystalline film phosphors, Crystals 11 (2021) 788, https://doi.org/10.3390/cryst11070788.

[33] Y. Zorenko, T. Zorenko, T. Voznyak, A. Mandowski, Q. Xia, M. Batentschuk, J. Friedrich, Luminescence of F+ and F centers in Al2O3-Y2O3 oxide compounds, IOP Conf. Ser. Mater. Sci. Eng. 15 (2010), 012060, https://doi.org/10.1088/1757-899x/15/1/012060.

[34] A. Pujats, M. Springis, The F-type centres in YAG crystals, Radiat. Eff. Defect Solid 155 (2001) 65–69, https://doi.org/10.1080/10420150108214094.